https://orcid.org/0000-0002-1873-1456
Kwaśniewski

INTERNATIONAL
Agrophysics
www.international-agrophysics.org

Int. Agrophys., 2026, 40, 321-337
doi: 10.31545/intagr/218363

Foliar application of chitosan-zinc oxide nanoparticles improved the yield of pea by modulating photosynthetic pigments, water status, and osmotic concentration under water stress**

Aqsa Malik[1,2], *Sumera Iqbal*[1]*, *Khajista Jabeen*[1], *Modhi O. Alotaibi*[3,4], *Aisha Umar*[5], *Lala Gurbanova*[6,7], *Muhammad Hayder Ali*[8], *Dariusz Kwaśniewski*[9], *Kholoud K. Alzahrani*[10], *Marek Gancarz*[9,11]*

[1]Department of Botany, Lahore College for Women University, 54000 Lahore, Pakistan
[2]Department of Botany, Faculty of Science, University of Narowal, 3-KM Shakargarh Road, Narowal 51600, Pakistan
[3]Department of Biology, College of Science, Princess Nourah bint Abdulrahman University, P.O. Box 84428, Riyadh 11671, Saudi Arabia
[4]Environmental and Biomaterial Unit, Natural and Health Sciences Research Center, Princess Nourah bint Abdulrahman University, Riyadh, Saudi Arabia
[5]Institute of Botany, University of the Punjab, Quaid-e-Azam Campus, 54590, Lahore, Pakistan
[6]Department of Life Sciences, Western Caspian University, University, Baku, Azerbaijan
[7]Department of Medical Biology and Genetics, Medical University, Baku, Azerbaijan
[8]College of Landscape Architecture, Department of Forestry, Sichuan Agricultural University, 611130, Chengdu, China
[9]Faculty of Production and Power Engineering, University of Agriculture in Kraków, Balicka 116B, 30-149 Kraków, Poland
[10]Department of Biology, University College of Umluj, University of Tabuk, Umluj, Tabuk, 46429, Saudi Arabia
[11]Institute of Agrophysics Polish Academy of Sciences, Doświadczalna 4, 20-290 Lublin, Poland

Received October 14, 2025; accepted February 20, 2026

A b s t r a c t. Among the various stresses affecting crop productivity, drought is a major challenge, particularly for leguminous crops like peas. The present study investigated the potential of chitosan-zinc oxide nanoparticles (CHT-ZnO NPs) to enhance drought tolerance in *Pisum sativum* L. through foliar application. The nanoparticles were synthesized *via* ion gelation, characterized before application using field emission scanning electron microscopy (FE-SEM), X-ray diffraction (XRD), Fourier transform infrared (FTIR), and X-ray photoelectron spectroscopy (XPS). Thereafter, CHT-ZnO NPs were applied to pea plants at concentrations of 200 ppm and 400 ppm as well as $ZnSO_4$ under different drought stress levels as per treatment plan. The results demonstrated that CHT-ZnO NPs significantly enhanced physiological and yield attributes of tested plant, even under moderate to severe drought stress. Notably, the 200 ppm dose of CHT-ZnO NPs showed the most significant improvement in chlorophyll contents (42.8 to 31.9%) and overall yield (54.6 to 43.2%), compared to their respective control under moderate to severe drought (60 and 40% field capacity (FC), respectively), thereby mitigating the adverse effects of drought. These findings suggest that the foliar application of CHT-ZnO NPs could become a promising strategy to improve drought resilience in pea crops.

K e y w o r d s: chitosan, drought stress, nanocomposites, *Pisum sativum*, yield, zinc oxide nanoparticles

*Corresponding author e-mail: marek.gancarz@urk.edu.pl
sumeraiqbal2@yahoo.com

**This work was funded by the Princess Nourah bint Abdulrahman University Researchers Supporting Project number (PNURSP2026R101), Princess Nourah bint Abdulrahman University, Riyadh,Saudi Arabia.

1. INTRODUCTION

The production of high-quality and nutrient-enriched food under the influence of climate change is a threatening challenge which requires a sustainable solution to ensure food security issues. It is estimated that the global population is projected to reach 9.7 billion by the end of 2025; therefore, it is the need of the hour to increase the existing food production by 70% to meet the rising food demand (Shahab *et al.*, 2024). Among abiotic stresses, drought is the most critical constraint which limits agricultural productivity (Jan *et al.*, 2025). Adverse climatic changes, like decreased precipitation, altered rainfall patterns, and increased temperature, are the main causes of global drought occurrence (Ishfaq *et al.*, 2025). In 2022, about 30% of the global land area was under moderate to extreme drought (Gebrechorkos *et al.*, 2025; Havii *et al.*, 2025). In Asia, around 1.7 billion hectares (from 4.3 billion hectares) of total land area is prone to drought stress due to their arid, semi-arid, or sub-humid climate (Nadeem *et al.*, 2019). In plants, drought stress adversely affects physiological processes, including photosynthesis, stomatal conductance,

rate of cell division and elongation, nutrient uptake, and membrane stability, resulting in decreased biomass accumulation and yield losses (Khan *et al.*, 2025). Hence, it is required to develop sustainable, resource-efficient, and eco-friendly strategies to mitigate the impacts of drought stress on plants.

Traditional agricultural intensification to meet global food demand heavily relies on agrochemicals such as fertilizers and pesticides, which pose serious environmental threats like soil degradation, groundwater contamination, and greenhouse gas emissions (Elumalai *et al.*, 2025). However, the recent development in nanotechnology offers innovative approaches to enhance crop resilience and productivity (Sharma *et al.*, 2025; Gorczyca *et al.*, 2024; Priss *et al.*, 2024). In recent years, the use of zinc oxide nanoparticles (ZnO NPs) has become very popular, as it improves the growth rate, physiology, and nutrient status of the existing crops and improves their nutritional values to mitigate malnutrition crises (Inam *et al.*, 2024). ZnO NPs, characterized by their nanoscale size (<100 nm), high surface area, and semiconductor properties, serve as bioavailable sources of zinc (Zn) (Mandal *et al.*, 2022, Gökmen *et al.*, 2024). It acts as an essential micronutrient involved in enzyme activation, protein synthesis, and chlorophyll formation in plants (Patel *et al.*, 2020). Numerous studies have also reported that CHT-ZnO NPs are generally recognized as safe (GRAS) and demonstrate efficacy in improving plant growth and tolerance to drought stress (Fatima *et al.*, 2024, Monib *et al.*, 2023).

Chitosan (CHT), derived from chitin, is a partially deacetylated polymer of N-acetyl glucosamine which possesses unique attributes such as biodegradability, biocompatibility, and a positive surface charge due to its amino groups (Ali *et al.*, 2024). Recently, chitosan has been described particularly as an elicitor of plant defense for plant protection (Stasińska-Jakubas and Hawrylak-Nowak, 2022). The synergistic application of CHT and ZnO NPs as chitosan-zinc oxide nanoparticles (CHT-ZnO NPs) is helpful for drought mitigation through enhanced antioxidant defense, improved nutrient uptake, and maintenance of cellular homeostasis (Rani *et al.*, 2024). Foliar-applied nanoformulations, in comparison with conventional fertilizers, do not require the root system and adequate topsoil moisture, thus providing a direct route for nutrient delivery to plants (Singh G.B. *et al.*, 2024). They also facilitate direct and rapid absorption through cuticular pores, stomata, or nano-scale penetration, while minimizing losses due to precipitation, adsorption, or immobilization in dry soils (Wang X. *et al.*, 2023). This route ensures rapid nanoparticle uptake at the primary sites of photosynthesis and induces plant defense mechanisms by activating antioxidant enzymes (in case of ROS production), osmolyte synthesis, and stomatal regulation. This synergistic effect is more effective when applied to leaves, where stress signaling occurs (Seleiman *et al.*, 2023).

Pea (*Pisum sativum* L.) is a major vegetable crop valued for its carbohydrates, proteins, vitamins, and essential amino acids such as lysine and tryptophan (Bagheri *et al.*, 2023). As a legume, it contributes to cereal-based rotations through nitrogen fixation, but its cultivation area has declined due to climate change and extreme weather such as drought (Kumar *et al.*, 2023). The crop is particularly vulnerable to drought stress, with the flowering stage being more sensitive than the vegetative phase (Bagheri *et al.*, 2023). Pea growth and yield in semi-arid regions have attracted considerable attention due to effect of climate change and water scarcity (Azmat *et al.*, 2024; Ocieczek *et al.*, 2025), which is why this crop was chosen for the study. Although the individual effects of chitosan and ZnO nanoparticles in enhancing plant stress tolerance have been reported, their integration into a single nanoformulation and foliar delivery has rarely been tested in legumes under field conditions. Previous studies mostly focused on either ZnO NPs or chitosan alone or evaluated their effects in controlled environments such as hydroponics or pot experiments. To our knowledge, no study has yet assessed the combined foliar application of chitosan-ZnO nanoparticles in pea (*Pisum sativum* L.) subjected to moderate and severe drought stress in field trials. The present work therefore provides novel insights into the synergistic role of CHT-ZnO NPs in improving growth, physiology, antioxidant defense, and yield attributes, while validating their potential as a sustainable strategy for climate-resilient legume production.

2. MATERIALS AND METHODS

2.1. Synthesis and characterization of chitosan-zinc oxide nanoparticles

The ion gelation method reported by Choudhary *et al.* (2019) was adopted with slight modifications for the synthesis of chitosan-zinc oxide nanoparticles (CHT-ZnO NPs). Briefly, low molecular weight chitosan was dissolved in 0.1% (v/v) acetic acid with continuous stirring; then, the pH was adjusted to 4.6-4.8 with 10N NaOH, and TPP was added drop-wise to this solution for cross-linking. Moreover, $ZnSO_4$ (0.02%, w/v) was added to prepare colloidal solutions. Dry powder of the nanocomposite was obtained by lyophilizing the gel using a freeze dryer (Heto Drywinner Freeze Dryer Model – CT/DW 60E). A portion of these lyophilized nanocomposites was subjected to calcination at 400°C for 2-3 h in air. The organic matrix decomposed, leaving behind crystalline ZnO nanoparticles, which facilitated the conversion of Zn^{2+} species into ZnO nanoparticles. Thereafter, for further characterization, pure chitosan (low molecular weight), ZnO nanoparticles, and CHT-ZnO NPs were stored at room temperature. Field emission scanning electron microscopy coupled with energy dispersive x-ray spectroscopy (Carl Zeiss VP500, operating voltage of 10 kV) was used to examine

the morphological and elemental composition of Chitosan, ZnO, and their composite materials. X-ray diffraction analysis was performed to determine the structural properties of pristine chitosan, pure ZnO nanostructures, and CHT-ZnO composites. For this purpose, utilized angle range of 10° to 70°, step size 0.02° s^{-1}, a Cu with Kα radiation source having wavelength 1.5409 Å was used to capture the spectra with a Bruker D8 advance X-beam diffractometer. FTIR analysis was conducted using a BRUKER TENSOR 27 spectrometer equipped with a smart strength single-bounce diamond ATR (attenuated total reflectance) cell. Spectral data were acquired in the range of 3700 cm^{-1} to 650 cm^{-1} with a resolution of 1 cm^{-1}, averaging 15 scans per sample. The acquired spectra were processed and analyzed using the GRAMS software package. An X-ray photoemission spectroscopy (XPS) PS system from Scienta-Omicron equipped with a monochromatic Al K-Alpha X-ray source (1486.7 eV) was employed for in-depth chemical analyses and determination of the surface chemistry composition of the composite. The operating conditions included a 700 μm spot size, analyzer energy (CAE) of 100 electron volts for general scan, and sources operating at 15 KeV. After Shirley background corrections, the spectra were fitted using the Gaussian-Lorentzia line shape. The XPS data were calibrated with C1s peak at 284.8 eV.

2.2. Experimental layout

The field experiment was conducted during the 2023/2024 growing season in sandy loam soil, at the Shakargarh (longitudes 32°15'38.7" N and longitudes 75°10'37.2" E) District, Narowal, Punjab, Pakistan, to evaluate the impact of foliar application of CHT-ZnO NPs on pea (*Pisum sativum* L. cv. Meteor) in field conditions under various drought levels. The soil samples were collected from various sites within the field area; then, a composite sample was prepared, and various physiochemical attributes of soil were measured following the standard protocols (Estefan *et al.*, 2013). The texture of the soil was sandy loam with 51% sand, 45% silt, and 04% clay. The other parameters included EC 4.5 dSm^{-1}, pH 7.7, total organic carbon 0.83%, organic matter 1.42%, sodium 1 586 mg kg^{-1}, Ca+Mg 17.2 meq L^{-1}, total phosphorus 0.027%, total potassium 0.38%, total zinc 64 mg kg^{-1}, total manganese 257 mg kg^{-1}, and total Fe 359 mg kg^{-1}.

The experiment was conducted under controlled conditions in terms of irrigation regime, foliar application rates, and experimental layout, while the soil type was determined by the natural field characteristics of the study site, as confirmed through prior soil analysis. Sandy loam represents the prevailing soil texture in the region and reflects the agronomic environment in which pea is cultivated locally. While soil physicochemical properties may influence the magnitude of crop responses, the study focuses on treatment-induced physiological responses under controlled field management conditions. Accordingly, the observed response patterns are expected to be applicable to comparable agro-ecological settings, although quantitative variation across different soil types cannot be excluded.

The field experiment was arranged using a split-plot design with irrigation regimes (*i.e.*, 80%, 60%, and 40% FC) as the main-plot factor and Zn treatments (*i.e.*, DI water, $ZnSO_4$, 200 ppm CHT–ZnO NPs, 400 ppm CHT–ZnO NPs) as the subplot factor. Each treatment combination was replicated thrice, and a total of 36 experimental units were made. The main plots (irrigation regimes) were randomly assigned within blocks, and the subplots (Zn treatments) were randomly allocated within each main plot. Blocking was based on field orientation to minimize soil heterogeneity effects. Each subplot measured 3.66 × 0.30 m with 0.30 m plant spacing. To determine the field capacity of the soil, the method outlined by Sparks *et al.* (1996) was employed. This method aids in understanding the soil water holding capacity, a critical aspect in assessing plant water availability and irrigation requirements. Certified pea seeds were sourced locally from Talib Fertilizers and Co., Ikhlas Pur Road, Shakargarh, District Narowal, Punjab, Pakistan, and an equal number of seeds were planted per plot. After seedling emergence, standard agronomic practices (weed, pest, and disease management) were applied as required. Thirty days after sowing, when the pea plants reached the 39 BBCH stage, various drought regimes, *i.e.*, control (80% field capacity), moderate drought (60% FC), and severe drought (40% FC), were imposed, maintained, and monitored daily with the help of a soil moisture meter (Lutron PMS-714), and irrigation volumes were adjusted accordingly to sustain the target FC levels for each treatment. After 10 days of maintaining the drought, foliar applications of $ZnSO_4$ (at the recommended dose) (Dhaliwal *et al.*, 2022), CHT-ZnO NPs 200 ppm, and 400 ppm, and deionized water (in the control) were applied at three-day intervals at the BBCH 51, BBCH 55, and BBCH 59 growth stages of pea plants as per treatment plan. The rationale behind using 200 ppm and 400 ppm CHT-ZnO NPs is based on the findings of our previous experiment (unpublished data). Briefly, a pot trial was conducted in controlled conditions in which CHT-ZnO NPs at 6.5, 12.5, 25, 50, 100, 200, and then 400 ppm were applied *via* soil, foliar, and soil + foliar modes and tested against similar drought regimes. Based on best performance in terms of physiological, growth, and yield parameters, the best two concentrations (CHT-ZnO NPs 200 ppm and 400 ppm) and the best method (foliar application) were used in this experiment to check their impacts on pea plants in field conditions. Then, after 10 days of the last foliar dose, various physiological attributes were measured. The plants were harvested after 120 days of experimentation.

2.3. Physiological attributes of pea plants

Various physiological attributes of pea plants were evaluated to check the impacts of the applied treatments under various drought regimes. From each replicate, three plants were randomly selected, and newly matured leaves from these plants were collected to determine chlorophyll *a*, chlorophyll *b*, total chlorophyll, carotenoid contents, sugar contents, proline contents, and relative water content.

2.4. Chlorophyll and carotenoid contents

Chlorophyll and carotenoid contents were quantified following the procedures of Arnon (1949) and Lichtenthaler and Wellburn (1983). Briefly, fresh leaf tissue (0.1 g) from each treatment was gently cleaned with water and dried with blotting paper. The samples were homogenized using a pestle and mortar, and pigments were extracted with 5 mL of 80% acetone. Then, the extracts were transferred into 15 mL falcon tubes, and centrifuged at room temperature for 5 min. The supernatant was collected, and absorbance was recorded at 663, 645, and 470 nm using a UV–visible spectrophotometer (BMS UV 2600). Chlorophyll *a*, chlorophyll *b*, total chlorophyll, and carotenoid contents were calculated using the following equations:

$$\text{Carotenoid contents} = [100\ A470 - 3.27\ (\text{chl } a) - 104\ (\text{chl } b)] / 227, \quad (1)$$

$$\text{Chlorophyll } a = 12.21\ (A663) - 2.81\ (A645)7, \quad (2)$$

$$\text{Chlorophyll } b = 20.13(A645) - 5.03\ (A663), \quad (3)$$

$$\text{Total chlorophyll} = 20.2\ (A645) - 8.02\ (A663). \quad (4)$$

2.5. Evaluation of sugar contents

Soluble sugar content in pea leaves was determined following the method of DuBois *et al.* (1956). Fresh leaf tissue (0.1 g) was homogenized in a pestle and mortar with 10 mL of distilled water and vortexed at 3000 rpm for 10 min. From the supernatant, 0.1 mL was mixed with 1 mL of 5% phenol and incubated at room temperature for 1 h. Subsequently, 5 mL of concentrated sulfuric acid was added, and absorbance was recorded at 420 nm using a UV–visible spectrophotometer. The sugar concentration in the samples was calculated from a glucose standard curve prepared with known concentrations.

2.6. Osmo-protectants and relative water contents

Proline content in pea leaves was estimated following the method of Bates *et al.* (1973). Briefly, fresh leaf tissues (0.1 g) were homogenized in 4 mL sulfosalicylic acid and transferred to falcon tubes, then refrigerated for 24 h and centrifuged at 3000 rpm for 5 min. The supernatant was mixed with 4 mL of acid ninhydrin reagent and incubated in a water bath at 100°C for 1 h. After cooling, 4 mL toluene was added, and the colored toluene phase (light to dark pink) was separated using a separating funnel. Absorbance was measured at 520 nm using a UV–visible spectrophotometer.

Relative water content (RWC) was determined following the method of Sairam *et al.* (2002). In brief, recently expanded leaves of pea plants were excised, blotted dry, and weighed immediately to record fresh weight (FW). The samples were then soaked in distilled water for 4 h at room temperature to attain full turgidity. Thereafter, the leaves were gently blotted and weighed to obtain turgid weight (TW). Subsequently, the same leaves were oven-dried at 70°C for 48 h to record dry weight (DW). The *RWC* was calculated using the following equation:

$$RWC = \frac{fresh\ mass - dry\ mass}{saturated\ mass - dry\ mass} 100. \quad (5)$$

2.7. Yield attributes

After 120 days of plantation, the pea plants were harvested, and various yield attributes were measured afterwards. The pod number per plant was recorded manually by randomly selecting three plants from each replication. Thereafter, seeds from each pod were calculated manually and the average was taken from each replicate. For the determination of hundred-seed weigh, all seeds collected from same replicate were mixed and 100 seeds were collected from each replicate on a random basis. Afterwards, the weight of a hundred seeds was measured using a portable weight balance. At the end, the yield per hectare was calculated from each treatment to show overall productivity under various conditions.

2.8. Statistical analysis

The experiment was laid out as a split-plot design with irrigation regimes (80, 60, and 40% field capacity) as the main plot factor and foliar treatment (DI water, $ZnSO_4$, 200 ppm CHT-ZnO, 400 ppm CHT-ZnO) as the subplot factor, with three replicates. Data were analyzed by two-way ANOVA to test the effects of irrigation, foliar treatment, and their interaction. Prior to analysis, normality and homogeneity of variances were evaluated using Shapiro-Wilk and Levene's tests, respectively, and data were log- or square-root-transformed when assumptions were violated. The correct error terms were used to test main-plot and subplot effects separately. Pairwise mean comparisons among individual treatment were performed using Tukey's HSD indicated significant effects ($p \leq 0.05$). Although replication was limited to three per treatment, which constrains field-level inference, this replication number is consistent with prior agronomic field studies under resource-limited conditions. Results are presented as mean ± SE, and significant differences are indicated by different letters. All statistical analyses were performed in Statistix 8.1 software.

The R packages in R software (4.5.0) FactoMineR, and factoextra were used to compute PCA. The optimal number of principal components was determined using the Kaiser criterion (eigenvalue >1) in combination with the cumulative explained variance approach. The PCA input matrix consisted of 12 rows and 11 variables. Prior to PCA, the input data were standardized (mean-centered and scaled to unit variance). The PCA was performed in R using the prcomp() function with the argument scale. = TRUE, ensuring that all variables contributed equally regardless of their original measurement units.

3. RESULTS

3.1. Field emission electron microscopy analysis

Figure 1 shows the FE-SEM images and conforming EDS spectra of pure ZnO and the Chitosan-ZnO composite. The FE-SEM image of pure ZnO (Fig. 1a) reveals a granular and clustered morphology, consisting of densely packed particles. This structure is characteristic of crystalline ZnO and suggests a relatively high surface area due to the small particle size and rough texture. In contrast, the FE-SEM image of the Chitosan-ZnO composite (Fig. 1c) displays a significantly transformed morphology. The surface appears more compact and layered, with larger and smoother structures, indicating the presence of chitosan. The ZnO nanoparticles seem to be embedded within or coated by the biopolymer matrix.

The EDS spectrum of pristine ZnO nanostructures (Fig. 1b) confirms the elemental composition, showing strong peaks corresponding to zinc (Zn) and oxygen (O), with weight percentages of 60.6 and 39.4%, correspondingly. The non-appearance of additional elements shows the good purity of the as-fabricated ZnO nanostructures. Meanwhile, the EDS spectrum of the Chitosan-ZnO composite (Fig. 1d) shows the presence of additional elements, namely carbon (C) and nitrogen (N), with weight percentages of 43.6 and 39.1%, respectively. These are attributed to the organic chitosan polymer. The zinc and oxygen content are significantly reduced to 10.6 and 6.8%, respectively, reflecting the lower ZnO loading and successful dispersion within the chitosan matrix. The presence of these elements confirms the successful formation of the Chitosan-ZnO composite and the integration of inorganic and organic phases without detectable impurities. The combined FE-SEM and EDS analyses clearly demonstrate the morphological transformation and compositional variation resulting from the formation of the Chitosan-ZnO composite, verifying the successful synthesis of a hybrid material.

3.2. X-Ray diffraction analysis

As chitosan is a natural biopolymer derived from chitin, it is greatly employed for water treatment due to its biocompatibility, biodegradability, and non-toxicity (Jiménez-Gómez and Cecilia, 2020). X-ray diffraction (XRD) was employed to investigate crystallinity and basic structural features of chitosan. The XRD pattern of pure chitosan is shown in Fig. 2c, which typically exhibits broad peaks, demonstrating a semi-crystalline or amorphous structure. A broad diffraction peak appeared around 2θ = 20°, corresponding to the crystalline region of chitosan, where as a less intense peak detected around 2θ = 10° is related to low ordered structures (Jia *et al.*, 2020). The span of the peaks represents the low degree of crystallinity of chitosan due to its uneven arrangement and intermolecular hydrogen bonding. The peak around 2θ~20° is typically assigned to the (110) reflection plane, demonstrating the orientation of the polymer chains. The XRD pattern of pure chitosan indicates its semi-crystalline nature, displaying characteristic peaks near 10 and 20°, which validate its identity and structural integrity. The XRD spectra of the as-produced

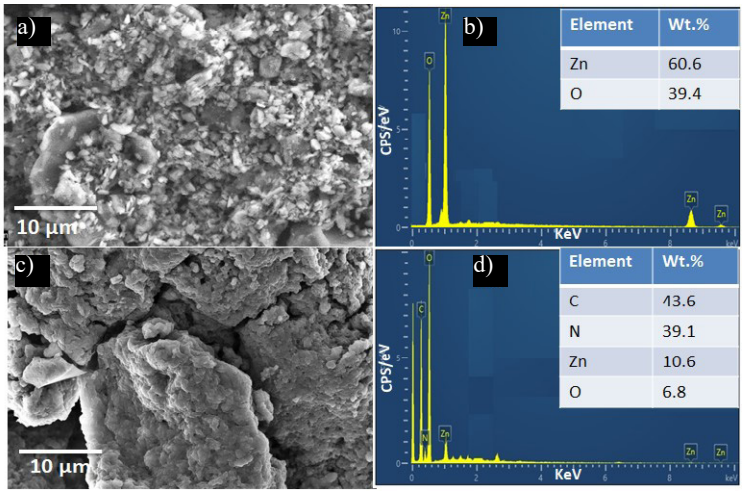

Fig. 1. Field emission scanning electron microscopy (FE-SEM) images with energy dispersive X-ray spectroscopy (EDS) spectrum: a) FE-SEM image of pure ZnO, b) EDS spectra of pristine ZnO nanostructures, c) FE-SEM image of the Chitosan-ZnO composite, d) EDS spectra of the Chitosan-ZnO composite.

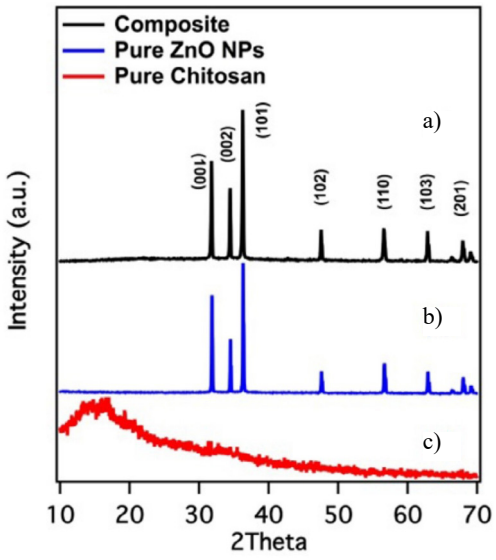

Fig. 2. XRD patterns of: a) the composite of Chitosan with ZnO structures, b) pure ZnO structures, and c) pure Chitosan.

a)

b)

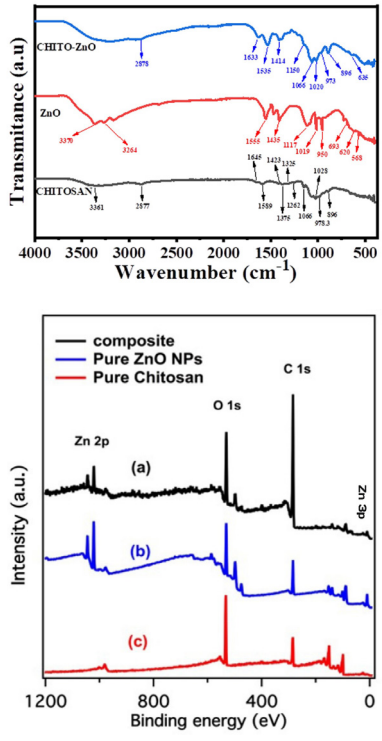

Fig. 3. FTIR spectra of: a) of the composite of Chitosan with ZnO structures (blue), pure ZnO NPs (red), and pure Chitosan (black); b) XPS survey spectra of: (a) the composite of Chitosan with ZnO structures (b) pure ZnO NPs, and (c) pure Chitosan.

ZnO nanostructures are presented in Fig. 2b. The XRD pattern displays prominent diffraction peaks that correspond to the hexangular wurtzite crystal ZnO nanostructure (JCPDS card no. 36-1451). The most intense regions are observed at 2θ values of approximately 31.8, 34.4, 36.3, 47.5, 56.6, 62.9, and 69.1°, which are indexed adjoining the (100), (002), (101), (102), (110), (103), and (201) atomic crystal planes, correspondingly. The most intense and well-defined nature of the Braggs peaks indicates the good lattice order of the ZnO structures (Yogamalar *et al.*, 2009; El-Khawaga *et al.*, 2025). No secondary peaks were detected, which may be related to impurities, confirming the high phase purity of the as-fabricated ZnO nanostructures. In Fig. 2a, the XRD patterns of the Chitosan-ZnO composite are depicted. This again shows the sharp and intense peaks representative of the hexagonal wurtzite phase of ZnO as in the case of pure ZnO structures (JCPDS card no. 36-1451) and the same main reflections observed. These peaks show the effective integration and high crystallinity of ZnO in the composite. The typical broad peaks of chitosan, normally observed around 10 and 20° are either absent or very weak in the composite (Sun *et al.*, 2025). This can be ascribed to the intrinsically low crystallinity of chitosan and its lower concentration relative to ZnO in the composite. Furthermore, the prime diffraction peaks from the highly crystalline ZnO phase expected overshadows the low diffraction component from the amorphous/semi-crystalline chitosan matrix. There are no additional peaks, which suggests that no secondary phases or impurities are present, confirming the successful fabrication of a phase-pure Chitosan-ZnO composite (Allah *et al.*, 2025).

3.3. FTIR analysis

The FTIR spectra of the composite of Chitosan with ZnO structures (blue), pure ZnO NPs (red), and pure Chitosan (black) are depicted in Fig. 3a. The IR spectra of pristine chitosan show a well-defined band region around 3 361 cm^{-1} related to O-H bonding, alongside the internal hydrogen bonding. The absorption band near 2 877 cm^{-1} is associated with the asymmetric stretching vibrations of C–H bonds. The existence of N-acetyl functionalities is evidenced by the characteristic peaks around 1 645 cm^{-1} (indicative of C=O stretching in amide I) and 1 325 cm^{-1} (corresponding to C–N stretching in amide III). A distinct peak at 1 589 cm^{-1} is linked to N–H bending vibrations typical of primary amine groups (Queiroz *et al.*, 2014). The deformation modes of CH_2 and the symmetric bending of CH_3 groups are reflected in the peaks observed around 1 423 and 1 375 cm^{-1}, respectively. Peaks at 1 066 and 1 028 cm^{-1} are assigned to C–O stretching vibrations. These spectral features are consistent with those documented for chitosan in previous studies (Queiroz *et al.*, 2014; Vino *et al.*, 2012; Song *et al.*, 2013). The signal appearing at 1 262 cm^{-1} is attributed to the bending motions of hydroxyl groups inherent in chitosan (Song *et al.*, 2013), while the band near 896 cm^{-1} is representative of out-of-plane CH bending related to the monosaccharide ring structure. The FTIR spectra of the synthesized zinc oxide nanoparticles were recorded in the range of 4 000-400 cm^{-1}. The spectrum exhibited characteristic bands corresponding to various functional groups at 3 370, 3 264, 3 160, 1 555, 1 435, 1 117,

1 019, 950, 693, 624, 620, and 568 cm^{-1}. The broad and intense peaks observed at 3 370 and 3 264 cm^{-1} are attributed to the asymmetric and symmetric stretching vibrations of hydroxyl (-OH) groups. The band near 1 555 cm^{-1} is assigned to the C=O stretching of the amide II group. A bending vibration associated with –C–H groups appears at 1 435 cm^{-1}. C–O stretching vibrations are identified at 1 117 and 1 019 cm^{-1}. The bending vibrations of =C–H groups manifest at 950 and 693 cm^{-1}, while the bending mode of O–H groups is evident at 620 cm^{-1}. Finally, the peak at 568 cm^{-1} corresponds to Zn–O bond stretching, confirming the successful formation of the zinc oxide nanoparticles (Mahalakshmi *et al*., 2020). The IR spectra of chitosan-ZnO show some combined peaks of ZnO and chitosan. In additional peaks, the absorption band at 1633 and 1535 cm^{-1} relates to the C=O group and stretching mode C=N, individually. The peaks at 1 414 and 1 150 cm^{-1} are attributed to C-N and C–O stretching vibrations, respectively. The peak in the composite appearing near 635 cm^{-1} is associated with the out-of-plane OH group (Movasaghi *et al.*, 2008).

3.4. X-ray photoelectron spectroscopy analysis

Figure 3b shows the survey scan of x-ray photoemission spectra (XPS), survey spectra of pure chitosan, pure ZnO NPs, and the composite of chitosan with ZnO NPs. The chitosan biopolymer primarily consists of such elements as carbon (C), oxygen (O), and nitrogen (N). Its XPS survey spectrum typically shows C 1s (~284.6 eV) associated with C–C/C–H bonding (aliphatic) and possibly C–O/C=O depending on the degree of deacetylation, Likewise, O 1s (~531–533 eV) and N 1s (~399–401 eV) peaks from hydroxyl and amine groups ($–NH_2$) are present in the survey spectrum, which depicts the purity of chitosan (Rinaudo, 2006). Similarly, in the figure, the second spectra correspond to pure ZnO nanoparticles. This spectrum typically shows Zn 2p (~1 021–1 045 eV) related to Zn $2p_{3/2}$ at ~1021.5 eV and Zn $2p_{1/2}$ at ~1044.5 eV due to orbit splitting. The O 1s peak around ~530.0-530.5 eV is attributed to lattice oxygen (O^{2-} in ZnO). The presence of carbon is associated with absorbed species from the surface (Baruah and Dutta, 2009). The XPS survey spectrum of the composite shows a combination of peaks from both Chitosan and ZnO. Specifically, C 1s is still present, possibly slightly shifted or broadened due to interactions with ZnO. The N 1s peak detected from Chitosan may exhibit a possible shift or change in intensity due to coordination with Zn^{2+}, and O 1s is more complex, as it includes the peaks from Zn–O (from ZnO) as well as C–O and O–H (from Chitosan) (Zaman *et al.*, 2022).

3.5. Photosynthetic pigments

In the present study, it was observed that the drought levels (*i.e*., 60 and 40% field capacity) exerted a significant impact on plant growth ($p \leq 0.05$) by altering its photosynthetic pigmentations. The DI treatment at 60% FC showed reduction of 24.2, 18.7, and 16.3% in Chl *a*, Chl *b*, and total chlorophyll in pea plants, respectively, compared to their respective control (DI 80% field capacity), as presented in Fig. 4. Similarly, in the case of the DI treatment at 40% FC, 40.1, 36.9 and 39.8% reduction in Chl *a*, Chl *b* and total chlorophyll of pea plants, respectively, was shown, compared to their respective control (DI 80% field capacity). However, in the case of 80% field capacity, the application of the Zn sources (in the form of $ZnSO_4$, 200 ppm CHT-ZnO NPs, and 400 ppm CHT-ZnO NPs) improved plant physiology and caused a substantial increase in Chl *a* (12.8, 50.4.7, and 25.6%), Chl *b* (18.7, 36.4, and 23.9%), and total chlorophyll (16.3, 42.2, and 24.6%), compared to their respective control (DI 80% field capacity).

Moreover, in the case of DI at 60% field capacity, the addition of $ZnSO_4$, 200 ppm CHT-ZnO NPs, and 400 ppm CHT-ZnO NPs increased Chl *a* (15.3, 67.2, and 50.6%), Chl *b* (12.4, 26.2, and 19.3%), and total chlorophyll (13.5, 42.8, and 31.9%), respectively, compared with their respective control (DI 60% field capacity). Additionally, in the treatments with severe drought stress, *i.e*., 40% field capacity, the application of $ZnSO_4$, 200 ppm CHT-ZnO NPs, and 400 ppm CHT-ZnO NPs caused a significant increase in Chl *a* (23.4, 69.2, and 43.9%, respectively), Chl *b* (22.1, 36.2, and 25.4%, respectively), and total chlorophyll (22.6, 49.7, and 33.0%, respectively), compared to their respective control (DI 40% field capacity).

In the present study, it was observed that the various drought levels, *i.e*., 60% and 40% field capacity, significantly impaired the chlorophyll contents (Chl *a*, Chl *b*, and total chlorophyll) in the pea plants. These results are consistent with the findings of (Pandey *et al.*, 2023), who also reported decreased chlorophyll contents and reduced photosynthetic rates of pea plants grown under drought stress. The decrease in chlorophyll contents might be linked with inhibited biosynthesis pathways, enhanced activities of chlorophyllase, and oxidative degradation of chlorophyll pigments due to reactive oxygen species (ROS) production and increased lipid peroxidation (Khayatnezhad and Gholamin, 2021; Sachdev *et al.*, 2021). This in turn decreases light harvesting and carbon fixation, which alters the physiological processes and impairs the growth and yield of pea plants (Pandey *et al.*, 2023; Khatun *et al.*, 2021).

However, the application of zinc in the form of nanoparticles improves the physiology of pea plants grown under drought stress (Mazhar *et al.*, 2023). The 200 ppm CHT-ZnO NP treatment exerted the most pronounced effects,

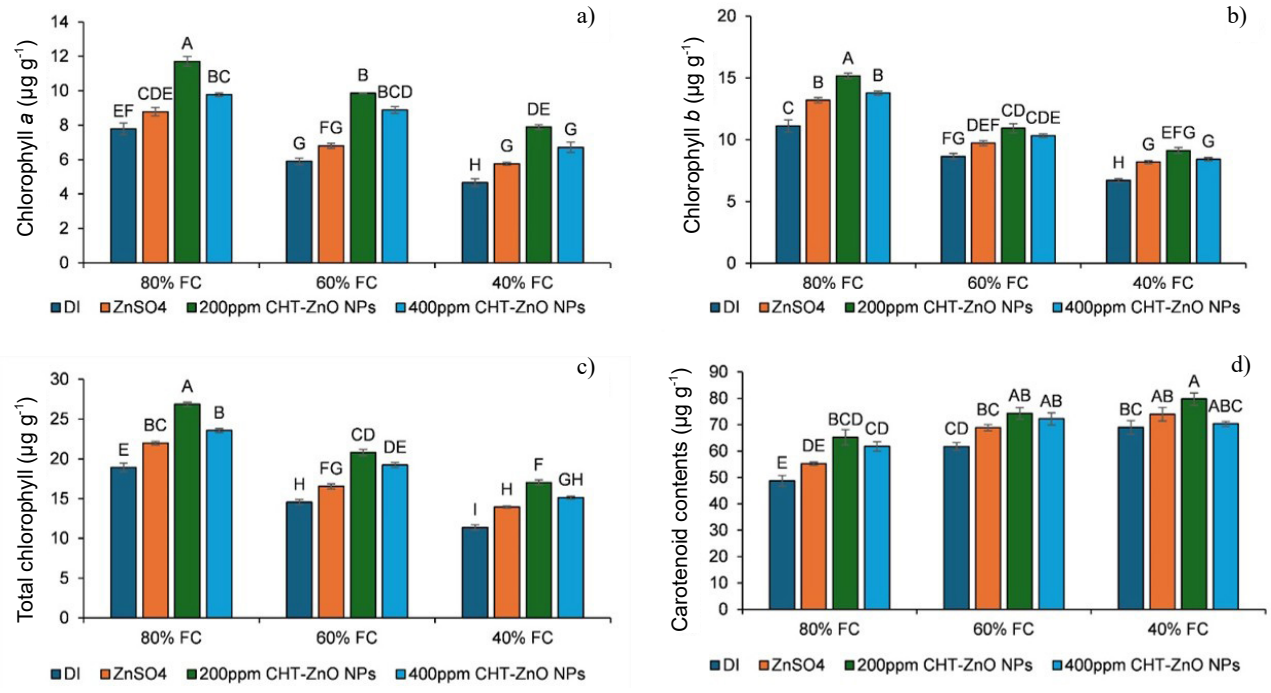

Fig. 4. Effects of various zinc sources on photosynthetic pigments: a) chlorophyll *a*, b) chlorophyll *b*, c) total chlorophyll, d) carotenoid contents in pea plants under various drought levels. Columns show the mean value of three replicates, while bars are standard errors. Columns sharing the same alphabet are not significantly different at $p<0.05$. FC – field capacity, NPs – nanoparticles.

compared to conventional $ZnSO_4$ and the 400 ppm NPs. Zinc plays a vital role in maintaining biomembrane structures and acts as a cofactor for various enzymatic activities such as carbonic anhydrase and chlorophyll synthetase (Balafrej *et al.*, 2020; Olayinka *et al.*, 2021). Both enzymes are pivotal in photosynthetic metabolism. The higher efficacy of CHT-ZnO NPs could be attributed to their improved penetration through leaf cuticles and stomatal openings to facilitate more efficient transport of nutrients to chloroplasts and enhance its reactivity and bioavailability (Avellan *et al.*, 2021; Rani *et al.*, 2023). Moreover, CHT-ZnO NPs could also indirectly regulate chlorophyll contents by mitigating oxidative damage to pigment-protein complexes in thylakoid membranes by enhancing the activity of antioxidant enzymes such as SOD, CAT, and POD (Raja *et al.*, 2024). These protective roles could collectively enhance photosynthetic efficiency and chlorophyll pigmentation even under moderate to severe drought stress.

While the current study showed an increase in carotenoid contents when the Zn treatments with $ZnSO_4$, 200 ppm CHT-ZnO NPs, and 400 ppm CHT-ZnO NPs were applied in all drought levels, as shown in Fig. 4. However, the treatment at 60 and 40% field capacity showed a significant increase of 26.6 and 41.5% in carotenoid contents, respectively, compared to the 80% field capacity. Moreover, within 80 and 60% of drought levels, the addition of $ZnSO_4$, 200 ppm CHT-ZnO NPs, and 400 ppm CHT-ZnO NPs caused an increase of 11.7 to 33.8% in carotenoid contents. However, the addition of the Zn sources did not show any significant improvement in carotenoid contents at 40% field capacity.

Carotenoids are very crucial in the plant photosystem due to their role in light harvesting and ROS scavenging ability (Simkin *et al.*, 2022). The observed increase in carotenoid content under moderate drought (60% FC) reflects an adaptative response aimed to minimize photo-oxidative stress, and the findings of the study are in line with the results described by Lima *et al.* (2018). The increase in carotenoid contents under the CHT-ZnO NP treatments, especially in the case of 200 ppm, supports that zinc not only facilitates structural stabilization of thylakoid membranes, but can also upregulate carotenoid biosynthetic genes such as phytoene synthase and lycopene β-cyclase (Li *et al.*, 2024).

In the present work, under 40% FC, the Zn treatments did not cause a further increase in carotenoid levels, which indicates their inability under severe drought stress. These results are in agreement with the findings of Saleem *et al.* (2024), who also observed a decrease in chlorophyll and carotenoid contents in pea plants under Cd toxicity. In severe drought, antioxidative machinery becomes overwhelmed and disturbs the plastidial metabolism and pigment synthesis (Singh A. *et al.*, 2024). This suggests that, under moderate conditions, CHT-ZnO NPs provide

robust protection. However, their efficiency is extremely compromised under extreme drought, which possibly inhibits nutrient uptake and causes cellular collapse.

3.6. Osmo-protectants and relative water contents

The present work showed a significant increase in sugar contents, *i.e.*, 52.6% under the moderate drought level (60% FC), compared to their respective control (DI 80% field capacity), as shown in Fig. 5. However, in the case of 40% field capacity, a significant decrease of 57.3% was observed in sugar contents, compared to their respective control. Moreover, the treatment with $ZnSO_4$, 200 ppm CHT-ZnO NPs, and 400 ppm CHT-ZnO NPs also produced a decrease of 69.2, 22.3, and 28.7%, respectively, compared to their respective controls. In the case of 80% field capacity, the addition of $ZnSO_4$, 200 ppm CHT-ZnO NPs, and 400 ppm CHT-ZnO NPs caused a significant increase of 65.3, 117, and 84.2%, respectively, in sugar contents, compared to their respective control (DI with 80% field capacity). Similarly, in the case of 60% field capacity, a significant increase of 31.8, 71.7, and 46.3% was observed upon the addition of $ZnSO_4$, 200 ppm CHT-ZnO NPs, and 400 ppm CHT-ZnO NPs, respectively, compared to their respective control (DI with 80% field capacity). Moreover, at 40% field capacity, the application of 200 ppm CHT-ZnO NPs and 400 ppm CHT-ZnO NPs caused a significant increase of 179 and 106%, respectively, in sugar contents, compared to their respective control (DI with 80% field capacity).

In the current work, the proline contents were significantly increased in moderate to severe drought stress. The proline contents increased by 103 to 185 at 60 and 40% field capacity, respectively, compared with the findings of the control (DI with 80% field capacity). However, the addition of the Zn sources caused a significant decrease in proline contents under various drought levels (as presented in Fig. 5). In the case of 80% field capacity, a significant decrease of 46.8, 147, and 60% in proline contents were observed under the application of $ZnSO_4$, 200 ppm CHT-ZnO NPs, and 400 ppm CHT-ZnO NPs, respectively, compared to their respective control (DI with 80% field capacity). Similarly, under 60% field capacity, a significant decrease of 22.1, 89.3, and 79.2% was observed upon the addition of $ZnSO_4$, 200 ppm CHT-ZnO NPs, and 400 ppm CHT-ZnO NPs, respectively, compared to their respective control (DI with 60% field capacity). Moreover, at 40% field capacity, the application of 200 ppm CHT-ZnO NPs and 400 ppm CHT-ZnO NPs caused a significant decrease of 82.4 and 60.6%, respectively, in proline contents, compared to their respective control (DI with 40% field capacity).

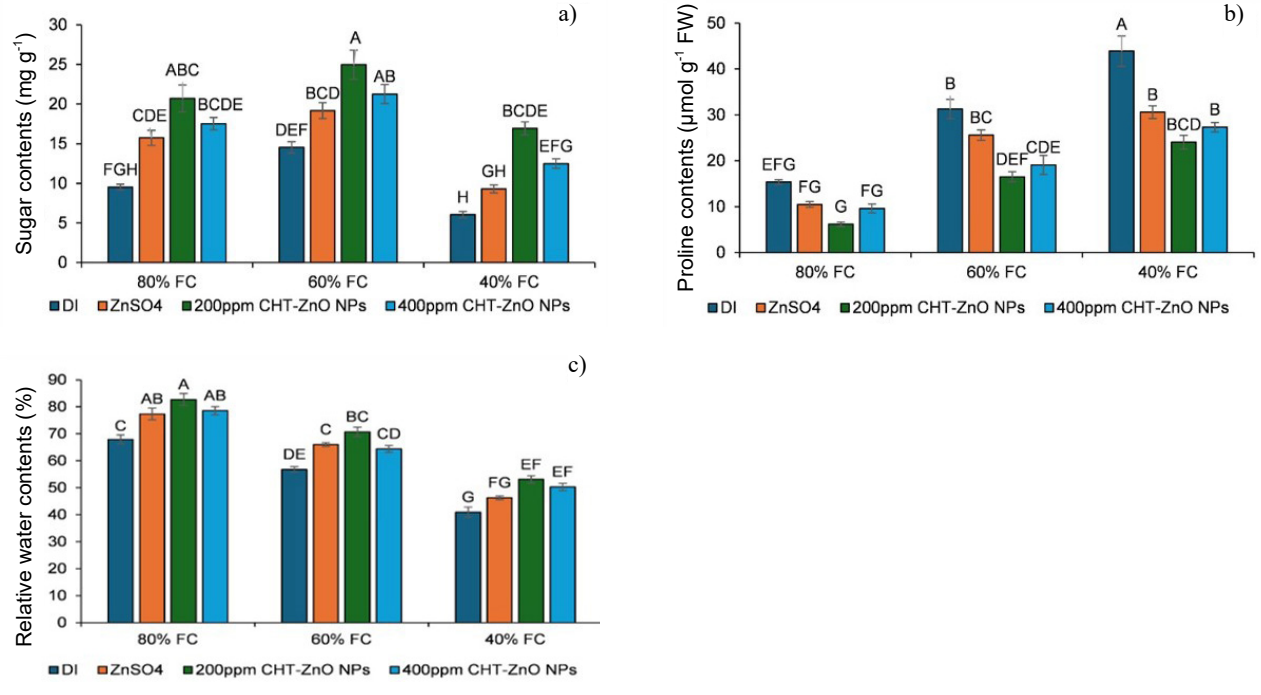

Fig. 5. Effects of various zinc sources on sugar contents (a), proline contents (b), and relative water contents (c) in pea plants under various drought levels. Columns show the mean value of three replicates, while bars are standard errors. Columns sharing the same alphabet are not significantly different at $p<0.05$. FC, field capacity; NPs, nanoparticles.

The relative water contents in the pea plants were significantly decreased under moderate to severe drought stress, *i.e*., 60 and 40% field capacity (Fig. 5). However, the addition of the Zn sources caused a moderate to significant increase in the relative water contents in the pea plants under various drought levels. In the case of 80% field capacity, a significant increase of 13.9, 21.8, and 15.7% in relative water contents were observed under the application of $ZnSO_4$, 200 ppm CHT-ZnO NPs, and 400 ppm CHT-ZnO NPs, respectively, compared to their respective control (DI with 80% field capacity), as shown in Fig. 5. Similarly, under 60% field capacity, a significant increase of 16.3, 24.6, and 13.4% was observed after the addition of $ZnSO_4$, 200 ppm CHT-ZnO NPs, and 400 ppm CHT-ZnO NPs, respectively, compared with their respective control (DI with 60% field capacity). Likewise, at 40% field capacity, the application of 200 ppm CHT-ZnO NPs, 400 ppm CHT-ZnO NPs, and $ZnSO_4$, caused a significant increase of 29.7, 22.9, and 13.0%, respectively, in relative water contents, compared to their respective control (DI with 40% field capacity).

In the present work, the sugar contents showed a dual response in terms of an increase under 60% FC and a drastic decline at 40% FC. This demonstrated the dynamic nature of osmotic adjustment in pea plants. Under moderate drought condition, carbohydrate metabolism becomes reactive to increase osmolyte accumulation, which enhances the osmotic potential and maintains cell turgidity (Singh *et al.*, 2023). Conversely, under higher drought stress, plant metabolism is adversely affected, limiting sugar biosynthesis and its mobilization (Ghani *et al.*, 2022).

The supplementation with 200 ppm CHT-ZnO NPs improved the sugar contents in the pea plants even at 40% FC. The present work supports the findings of Ajmal *et al.* (2023) and Semida *et al.* (2021), who also reported an increase in sugar contents in pea plants grown under drought stress and supplemented with ZnO NPs. This suggests that Zn plays a regulatory role in carbohydrate metabolism. Zn activates various enzymes like aldolase and invertase, which are crucial in glycolysis and sucrose cleavage, and thereby ensure continuous sugar supply for osmotic regulation (Singh A. *et al.*, 2024). The improved sugar levels under CHT-ZnO NP treatment could enhance carbon fixation, which is related to restoration of chlorophyll content and photosynthetic activities even under extreme drought stress (Sun *et al.*, 2021).

Similarly, proline contents are increased in drought stress. Proline is a key osmoprotectant and ROS scavenger, and its higher accumulation in plants is a hallmark of stress perception and cellular defense (Zulfiqar and Ashraf, 2023). Interestingly, the application of CHT-ZnO NPs decreased proline levels across moderate to severe drought conditions. This reduction signifies that the CHT-ZnO NPs-treated plants experienced lower oxidative and osmotic stress, thereby reducing the need for proline biosynthesis (Sadati *et al.*, 2022). In stress conditions, stress-inducible genes like *P5CS* and *OAT* become active and regulate proline synthesis. However, the application of Zn reduced the activation of these enzymes and improved the physiological status by upregulating proline dehydrogenase (which is crucial in catalyzing proline degradation) (Zulfiqar *et al.*, 2020). The reduction in proline might not only reflect decreased stress but could also represent metabolic reallocation or trade-offs. Since Zn is an integral part of protein and amino acid metabolism, it may shift nitrogen partitioning away from proline towards other amino acids or protein synthesis pathways (Ahmed *et al.*, 2024). Moreover, CHT-ZnO NPs may enhance carbon-nitrogen metabolism and stabilize membranes, thereby decreasing the necessity for excessive proline accumulation as a stress signal (Methela *et al.*, 2023). Such responses suggest that lower proline contents in plants under Zn application do not serve as an indicator of a weakened defense, but rather a reprogramming of metabolic priorities under improved physiological homeostasis.

In the present work, the relative water contents in the plants decreased under abiotic stress, and the findings are in line with the results of Ali *et al.* (2023), who also observed a decrease in relative water contents in chickpea plants subjected to abiotic stress. The reduced relative water contents measured in the study might be due to the stomatal closure, reduced water uptake, and cell wall stiffening in pea plants (Roig-Oliver *et al.*, 2021). The inclusion of ZnO NPs improved relative water contents, which might be due to enhanced root water conductivity through aquaporin regulation, stabilization of membrane lipids to prevent water loss, and activation of hormonal pathways like ABA signaling to modulate stomatal behavior and root growth (Singh A.*et al.*, 2024, Ahmed *et al.*, 2022). CHT-ZnO NPs enhance the plant's capacity to retain water and maintain cell expansion under water-deficient conditions.

3.7. Yield attributes

In the present study, it was observed that the drought levels (*i.e*., 60% and 40% field capacity) exerted a significant impact ($p \leq 0.05$) on the yield attributes of pea plants. The treatment at 60% field capacity showed a reduction of 43.4, 26.7, 25.6, and 25.3% in the number of pods, number of seeds, hundred-seed weight, and yield per hectare, respectively, compared to their respective control (DI 80% field capacity), as presented in Fig. 6. Similarly, in the case of the treatment at 40% FC, the analyses showed 64.2, 55.2, 60.4, and 60.3% reduction in the number of pods, number of seeds, hundred-seed weight, and yield per hectare, respectively, compared to their respective control (DI 80% field capacity). However, in the case of 80% field capacity, the application of the Zn sources (in the form of $ZnSO_4$, 200 ppm CHT-ZnO NPs, and 400 ppm CHT-ZnO NPs) improved the yield attributes of pea plants and caused a substantial increase in the number of pods (43.4,

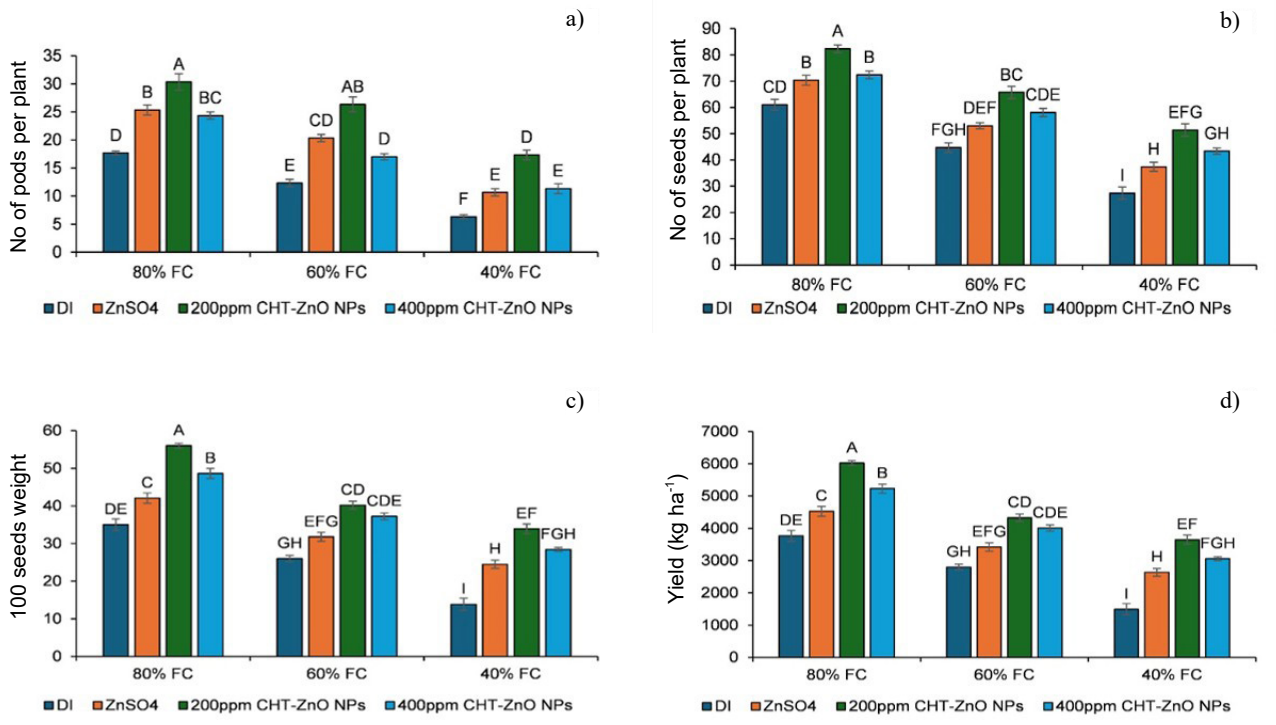

Fig. 6. Effects of various zinc sources on the number of pods per plant (a), number of seeds per plant (b), hundred seeds weight (c), and yield (d) of pea plants under various drought levels. Columns show the mean value of three replicates, while bars are standard errors. Columns sharing the same alphabet are not significantly different at $p < 0.05$. FC, field capacity; NPs, nanoparticles.

71.7, and 37.7%), number of seeds (15.3, 34.9, and 18.6%), hundred-seed weight (16.8, 37.4, and 27.9%), and yield per hectare (20.2, 59.9, and 38.6%), compared to their respective control (DI 80% field capacity). Moreover, in the case of DI at 60% field capacity, the addition of $ZnSO_4$, 200 ppm CHT-ZnO NPs, and 400 ppm CHT-ZnO NPs increased the number of pods (64.9, 113, and 37.8%), number of seeds (18.7, 47.0, and 29.9%), hundred-seed weight (18.1, 35.3, and 30.1%), and yield per hectare (22.1, 54.6, and 43.2%), respectively, compared with their respective control (DI 60% field capacity). Additionally, the treatments with severe drought stress, *i.e.*, 40% field capacity, the application of $ZnSO_4$, 200 ppm CHT-ZnO NPs, and 400 ppm CHT-ZnO NPs caused a significant increase in the number of pods (68.4, 174, and 78.9%, respectively), number of seeds (36.6, 87.8, and 58.5%, respectively), hundred-seed weight (43.4, 59.1, and 51.2%, respectively), and yield per hectare (76.7, 144, and 105%), compared to their respective control (DI 40% field capacity).

The reduction in yield under drought stress in the present work supports the findings of Kausar *et al.* (2023), who also observed a decline in overall grain seeds (yield) of pea plants under drought stress. This reduction is directly associated with impaired photosynthetic processes, reduced flowering, and low nutrient uptake. The decline in pods, seeds, and yield at both 60 and 40% FC highlight the cumulative effect of impaired source-sink relationships, oxidative damage, and hormonal imbalance under water stress (Nadeem *et al.*, 2019). Zinc is crucial for enzymatic functions involved in ATP synthesis and energy transfer, which are essentially important in the grain-filling phase by the conversion of photosynthates into storage compounds in the grains (Teng *et al.*, 2023; Suganya *et al.*, 2020). Zinc treatments, particularly with 200 ppm CHT-ZnO NPs, improved yield attributes across all conditions. This could be possible due to restoration of physiological processes, including improved photosynthesis, enhanced sugar and nutrient transport, and stabilization of reproductive structures (Wang Z. *et al.*, 2023). The enhanced photosynthesis during the grain-filling stage ensures a steady supply of nutrients and photosynthates to the developing grains, contributing to higher grain weight and overall yield (Raza *et al.*, 2025). Zinc plays a key role in pollen viability, auxin biosynthesis, and seed development, all of which are crucial under drought stress (Kandil *et al.*, 2022). Additionally, CHT-ZnO NPs enhance root architecture to assimilate nutrients along with water and contribute further to improving grain filling and overall plant yield (Dimkpa *et al.*,

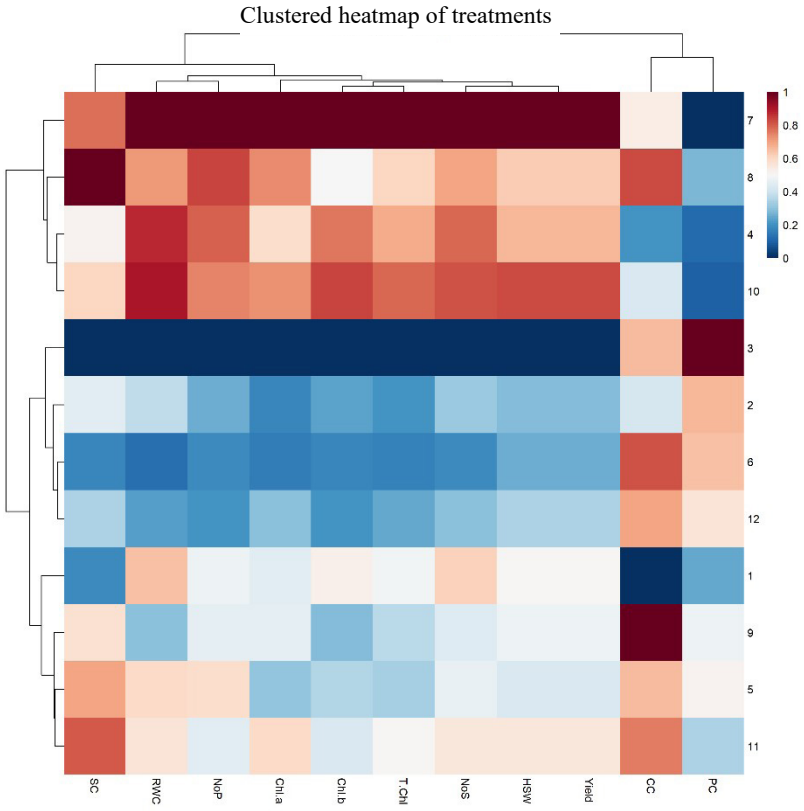

Fig. 7. Clustered heatmap indicating the relations between treatments and physiological and yield parameters in *Pisum sativum* L. Rows present treatments and column show parameters: chlorophyll contents (Chl. *a*, Chl. *b*, T. Chl), carotenoid contents (CC), sugar contents (SC), proline contents (PC), relative water contents (RWC), number of pods per plant (NoP), 100-seed weight (HSW), and yield. The intensity of colour indicates the magnitude of each parameter (red = high, blue = low).

2019). In the present study, the higher CHT-ZnO NPs dose (400 ppm) showed less benefits, compared to the 200 ppm treatment. The reasons for their limited role in plant growth might be due to nanoparticle aggregation, potential phytotoxicity, or interference with nutrient uptake (Sheteiwy *et al.*, 2021). Hence, careful optimization of nanoparticle concentration is helpful to avoid antagonistic effects and to improve crop yield in a sustainable way.

The application of CHT-ZnO NPs on pea plants improved the overall plant growth, physiology, and yield attributes and mitigated the impacts of abiotic stress on various plant growth stages. This could be a better strategy for sustainable agricultural production and food security while focusing on some limitations as well. The study was limited to a single crop and location, and responses may vary across different agro-ecological zones. Moreover, while chitosan carriers are biodegradable, the long-term environmental fate of ZnO NPs and their effects on soil health remain unclear. Likewise, the scalability and cost-effectiveness of large-scale CHT-ZnO NP production require further evaluation compared with conventional Zn fertilizers. Therefore, future work should include multi-crops, multi-location trials, and cost-benefit ratios to ensure safe and sustainable application. Further research should also be done on genetic level variations in pea plants induced by the supplementation of CHT-ZnO NPs for the assurance of sustainable food supplies.

3.8. Correlation matrix and principal component analysis

A clustered heatmap was generated to highlight the interaction between the twelve treatments and the measured physiological and yield attributes (Fig. 7). Treatments were grouped based on similarity in results across parameters, *i.e.*, chlorophyll contents (Chl *a*, Chl *b*, T.Chl), carotenoid contents (CC), sugar contents (SC), proline contents (PC), relative water contents (RWC), number of pods per plant (NoP), 100-seed weight (HSW), and yield. Treatments with CHT-ZnO NPs at 200 ppm and 400 ppm at field 80% FC tended to cluster together and showed higher chlorophyll contents, yield, and related physiological parameters indicated in red hues. On the other hand, the treatment under DI at 40% FC, without any addition, clustered separately and showed reduced values (blue) across most of the parameters. Notably, the clustering analysis showed that the application of 200 ppm CHT-ZnO NPs at 80% FC (treatment 7)

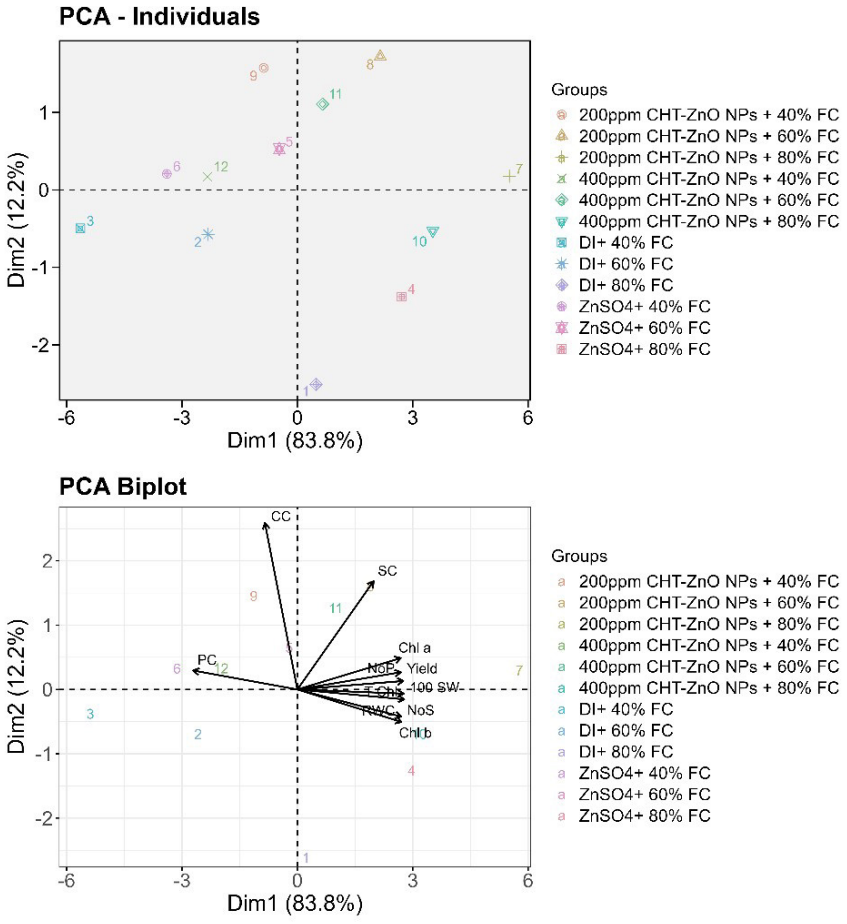

Fig. 8. PCA individual plots showing the distribution of different treatment groups, PCA biplot illustrating correlations between different physiochemical and yield parameters with different treatment groups.

was linked with the best overall performance, especially in terms of chlorophyll contents and yield, showing a synergistic effect of the NP treatment.

Principal component analysis (PCA) was performed to analyze the variation between the treatments. PC1 alone accounts for 83.8% of the variance, while PC2 accounts for 12.2% (Fig. 8). The PCA individual plot showed clear separation among the treatments. The PCA biplot showed that physiological parameters, such as sugar content (SC), Chlorophyll *a* (Chl *a*), Chlorophyll *b* (Chl *b*), and yield were the main contributors to PC1, positively influencing treatments located on the right side of the plot.

4. CONCLUSIONS

Chitosan-zinc oxide nanoparticles (CHT-ZnO NPs), synthesized via ion gelation and characterized through physicochemical analyses, demonstrated positive effects on pea (*Pisum sativum* L.) grown under drought conditions. Foliar applications, particularly at 200 ppm, improved physiological traits such as chlorophyll content, carotenoids, sugars, proline regulation, and relative water content, while also enhancing yield-related attributes under moderate drought stress (*i.e.*, 60% FC). These results suggest that CHT-ZnO NPs have potential as a promising tool to alleviate drought-induced damage in legumes. However, the present results are based on a single short-term field trial with limited replication and should therefore be interpreted cautiously. Long-term, multi-location studies are required to validate their effectiveness, assess scalability and cost-benefit ratios, and evaluate possible ecological or toxicological implications before widespread adoption in sustainable agriculture.

Authors Contributions: Conceptualization, AM, SI, KJ; methodology, AM, SI, KJ, AU,; software, MOA, SI, KJ; validation, KJ, AU, KKA, LG; investigation, MOA, MG; resources, AU, SI; writing original draft preparation, AM, AU, KJ, MHA, All authors, writing review and editing, AU, LG; supervision, SI, MG, MOA, KJ. All authors have read and agreed to the published version of the manuscript.

Collection of Plant Material/seeds: The meteor seeds used in this study were obtained from the local Shakargarh seed shop. Seeds were collected/purchased from Talib

Fertilizers and Co. Iklaspur Road, Shakargarh (longitudes 32°15’38.7”N and longitudes 75°10’37.2”E) District, Narowal, Punjab, Pakistan.

Data Availability Statement: The datasets used and/or analyzed during the current study are available from the corresponding author upon reasonable request.

Conflicts of Interest: The authors declare no conflicts of interest.

5. REFERENCES

Ahmed, M., Decsi, K. and Tóth, Z., 2022. Different tactics of synthesized zinc oxide nanoparticles, homeostasis ions, and phytohormones as regulators and adaptatively parameters to alleviate the adverse effects of salinity stress on plants. Life 13(1), 73. https://doi.org/10.3390/life13010073

Ahmed, M., Marrez, D.A., Rizk, R., Zedan, M., Abdul-Hamid, D., Decsi, K., *et al*., 2024. The influence of zinc oxide nanoparticles and salt stress on the morphological and some biochemical characteristics of *Solanum lycopersicum* L. plants. Plants 13(10), 1418. https://doi.org/10.3390/plants13101418

Ajmal, M., Ullah, R., Muhammad, Z., Khan, M.N., Kakar, H.A., Kaplan, A., *et al*., 2023. Kinetin capped zinc oxide nanoparticles improve plant growth and ameliorate resistivity to polyethylene glycol (PEG)-induced drought stress in *Vigna radiata* (L.) R. Wilczek (Mung Bean). Molecules 28(13), 5059. https://doi.org/10.3390/molecules28135059

Ali, G., Sharma, M., Salama, E.S., Ling, Z., Li, X., 2024. Applications of chitin and chitosan as natural biopolymer: potential sources, pretreatments, and degradation pathways. Biomass Convers. Biorefinery 14(4), 4567-4581. https://doi.org/10.1007/s13399-022-02684-x

Ali, M.H., Khan, M.I., Naveed, M., Tanvir, M.A., 2023. Microbe-assisted rhizoremediation of hydrocarbons and growth promotion of chickpea plants in petroleum hydrocarbons-contaminated soil. Sustainability 15(7), 6081. https://doi.org/10.3390/su15076081

Allah, M.A.A.H., Ibrahim, H.K., Abdulridha, A.A., 2025. Eco-friendly synthesis of ZnO/chitosan nanocomposite: Detailed characterization, DFT study, docking study, adsorption kinetics, thermodynamic analysis and antioxidant properties. J. Mol. Liq. 425, 127216. https://doi.org/10.1016/j.molliq.2025.127216

Arnon, D.I., 1949. Copper enzymes in isolated chloroplasts. Polyphenoloxidase in Beta vulgaris. Plant Physiol. 24(1), 1. https://doi.org/10.1104/pp.24.1.1

Avellan, A., Yun, J., Morais, B.P., Clement, E.T., Rodrigues, S.M. Lowry, G.V., 2021. Critical review: role of inorganic nanoparticle properties on their foliar uptake and in planta translocation. Environ. Sci. Technol. 55(20), 13417-13431. https://doi.org/10.1021/acs.est.1c00178

Azmat, M., Haider, S., Mahmood, M.H., Siddiqa, F., Ammara, G., Rehman, A.U., *et al.*, 2024. Evaluation of yield, growth potential and adaptability of ten pea lines under semi-arid conditions. Planta Animalia 3(2), 97-106.

Bagheri, M., Santos, C.S., Rubiales, D., Vasconcelos, M.W., 2023. Challenges in pea breeding for tolerance to drought: Status and prospects. Ann. Appl. Biol. 183(2), 108-120. https://doi.org/10.1111/aab.12840

Balafrej, H., Bogusz, D., Triqui, Z.E.A., Guedira, A., Bendaou, N., Smouni, A., *et al*., 2020. Zinc hyperaccumulation in plants: A review. Plants 9(5), 562. https://doi.org/10.3390/plants9050562

Baruah, S., Dutta, J., 2009. Hydrothermal growth of ZnO nanostructures. Sci. Technol. Adv. Mate. 10(1), 013001. https://doi.org/10.1088/1468-6996/10/1/013001

Bates, L.S., Waldren, R.P.A., Teare, I.D., 1973. Rapid determination of free proline for water-stress studies. Plant Soil 39(1), 205-207. https://doi.org/10.1007/BF00018060

Choudhary, R.C., Kumaraswamy, R.V., Kumari, S., Sharma, S.S., Pal, A., Raliya, R., *et al*., 2019. Zinc encapsulated chitosan nanoparticle to promote maize crop yield. Int. J. Biol. Macromol. 127, 126-135. https://doi.org/10.1016/j.ijbiomac.2018.12.274

Dhaliwal, S.S., Sharma, V., Shukla, A.K., Kaur, J., Verma, V., Kaur, M., *et al*., 2022. Zinc-based mineral ($ZnSO_4 \cdot 7H_2O$) and chelated (Zn-EDTA) fertilizers improve the productivity, quality and efficiency indices of field pea (*Pisum sativum* L.) through biofortification. J. Trace Elem. Miner. 2, 100033. https://doi.org/10.1016/j.jtemin.2022.100033

Dimkpa, C.O., Singh, U., Bindraban, P.S., Elmer, W.H., Gardea-Torresdey, J.L., White, J.C., 2019. Zinc oxide nanoparticles alleviate drought-induced alterations in sorghum performance, nutrient acquisition, and grain fortification. Sci. Total Environ. 688, 926-934. https://doi.org/10.1016/j.scitotenv.2019.06.392

DuBois, M., Gilles, K.A., Hamilton, J.K., Rebers, P.A., Smith, F., 1956. Colorimetric method for determination of sugars and related substances. Anal. chem. 28(3), 350-356. https://doi.org/10.1021/ac60111a017

El-Khawaga, A.M., Elsayed, M.A., Gobara, M., Suliman, A.A., Hashem, A.H., Zaher, A.A., *et al*., 2025. Green synthesized ZnO nanoparticles by Saccharomyces cerevisiae and their antibacterial activity and photocatalytic degradation. Biomass Convers. Biorefinery 15(2), 2673-2684. https://doi.org/10.1007/s13399-023-04827-0

Elumalai, P., Gao, X., Parthipan, P., Luo, J., Cui, J., 2025. Agrochemical pollution: A serious threat to environmental health. Curr. Opin. Environ. Sci. Health 100597. https://doi.org/10.1016/j.coesh.2025.100597

Estefan, G., Sommer, R., Ryan, J., 2013. Methods of Soil, Plant, and Water Analysis: A manual for the West Asia and North African region (Third Edition). Int. Cent. Agric. Res. Dry Areas.

Fatima, A., Zaheer, T., Pal, K., Abbas, R.Z., Akhtar, T., Ali, S., *et al*., 2024. Zinc oxide nanoparticles significant role in poultry and novel toxicological mechanisms. Biol. Trace Elem. Res. 202(1), 268-290. https://doi.org/10.1007/s12011-023-03651-x

Gebrechorkos, S.H., Sheffield, J., Vicente-Serrano, S.M., Funk, C., Miralles, D.G., Peng, J., *et al*., 2025. Warming accelerates global drought severity. Nature 1-8. https://doi.org/10.1038/s41586-025-09047-2

Ghani, M.I., Saleem, S., Rather, S.A., Rehmani, M.S., Alamri, S., Rajput, V.D., *et al*., 2022. Foliar application of zinc oxide nanoparticles: An effective strategy to mitigate drought

stress in cucumber seedling by modulating antioxidant defense system and osmolytes accumulation. Chemosphere 289, 133202. https://doi.org/10.1016/j.chemosphere.2021.133202

Gorczyca, A., Przemieniecki, S.W., Oćwieja, M., 2024. Comparative effect of silver nanoparticles on maize rhizoplane microbiome in initial phase of plants growth. Int. Agrophys. 38(2), 155-164. https://doi.org/10.31545/intagr/184863

Gökmen, G.G., Mirsafi, F.S., Leißner, T., Akan, T., Mishra, Y.K. Kışla, D., 2024. Zinc oxide nanomaterials: Safeguarding food quality and sustainability. Comp. Rev. Food Sci. Food Saf. 23(6), 70051. https://doi.org/10.1111/1541-4337.70051

Havii, V., Palyvoda, Y., Kuchmenko, O., Stamirowska-Krzaczek, E., Tomaszewska, M., Kocira, A., 2025. Biochemical mechanisms of drought resistance in soft wheat under modeling of water deficiency and effects of seed treatment with metabolically active substances. Agric. Eng. 29(1), 15-31. https://doi.org/10.2478/agriceng-2025-0002

Inam, A., Javad, S., Naseer, I., Alam, P., Almutairi, Z.M., Faizan, M., *et al*., 2024. Efficacy of chitosan loaded zinc oxide nanoparticles in alleviating the drastic effects of drought from corn crop. Plant Stress 14, 100617. https://doi.org/10.1016/j.stress.2024.100617

Ishfaq, A., Haidri, I., Shafqat, U., Khan, I., Iqbal, M., Mahmood, F., *et al*., 2025. Impact of biogenic zinc oxide nanoparticles on physiological and biochemical attributes of pea (*Pisum sativum* L.) under drought stress. Physiol. Mol. Biol. Plants 31(1),11-26. https://doi.org/10.1007/s12298-024-01537-3

Jan, M.F., Altaf, M.T., Liaqat, W., Liu, C., Mohamed, H.I., Li, M., 2025. Approaches for the amelioration of adverse effects of drought stress on soybean plants: from physiological responses to agronomical, molecular, and cutting-edge technologies. Plant Soil 1-53. https://doi.org/10.1007/s11104-025-07202-2

Jia, Z., Yang, C., Zhao, F., Chao, X., Li, Y., Xing, H., 2020. One-step reinforcement and deacidification of paper documents: Application of Lewis base-Chitosan nanoparticle coatings and analytical characterization. Coatings 10(12), 1226. https://doi.org/10.3390/coatings10121226

Jiménez-Gómez, C.P., Cecilia, J.A., 2020. Chitosan: a natural biopolymer with a wide and varied range of applications. Molecules 25(17), 3981. https://doi.org/10.3390/molecules25173981

Kandil, E.E., El-Banna, A.A., Tabl, D.M., Mackled, M.I., Ghareeb, R.Y., Al-Huqail, A.A., *et al*., 2022. Zinc nutrition responses to agronomic and yield traits, kernel quality, and pollen viability in rice (*Oryza sativa* L.). Front. Plant Sci. 13, 791066. https://doi.org/10.3389/fpls.2022.791066

Kausar, A., Zahra, N., Zahra, H., Hafeez, M.B., Zafer, S., Shahzadi, A., *et al*., 2023. Alleviation of drought stress through foliar application of thiamine in two varieties of pea (*Pisum sativum* L.). Plant Signal. Behav. 18(1), 2186045. https://doi.org/10.1080/15592324.2023.2186045

Khan, A.A., Wang, Y.F., Akbar, R., Alhoqail, W.A., 2025. Mechanistic insights and future perspectives of drought stress management in staple crops. Front. Plant Sci. 16, 1547452. https://doi.org/10.3389/fpls.2025.1547452

Khatun, M., Sarkar, S., Era, F.M., Islam, A.M., Anwar, M.P., Fahad, S., *et al*., 2021. Drought stress in grain legumes: Effects, tolerance mechanisms and management. Agronomy 11(12), 2374. https://doi.org/10.3390/agronomy11122374

Khayatnezhad, M., Gholamin, R., 2021. The effect of drought stress on the superoxide dismutase and chlorophyll content in durum wheat genotypes. Adv. Life Sci. 8(2), 119-123. https://doi.org/10.62940/als.v8i2.1066

Kumar, S., Gopinath, K.A., Sheoran, S., Meena, R.S., Srinivasarao, C., Bedwal, S., *et al*., 2023. Pulse-based cropping systems for soil health restoration, resources conservation, and nutritional and environmental security in rainfed agroecosystems. Front. Microbiol. 13, 1041124. https://doi.org/10.3389/fmicb.2022.1041124

Li, Y., Zheng, L., Mustafa, G., Shao, Z., Liu, H., Li, Y., *et al*., 2024. Enhancing post-harvest quality of tomato fruits with chitosan oligosaccharide-zinc oxide nanocomposites: A study on biocompatibility, quality improvement, and carotenoid enhancement. Food Chem. 454, 139685. https://doi.org/10.1016/j.foodchem.2024.139685

Lichtenthaler, H.K., Wellburn, A.R., 1983. Determinations of total carotenoids and chlorophylls *a* and *b* of leaf extracts in different solvents. https://doi.org/10.1042/bst0110591

Lima, C.S., Ferreira-Silva, S.L., Carvalho, F.E.L., Neto, M.C.L., Aragão, R.M., Silva, E.N., *et al.*, 2018. Antioxidant protection and PSII regulation mitigate photo-oxidative stress induced by drought followed by high light in cashew plants. Environ. Exp. Bot. 149, 59-69. https://doi.org/10.1016/j.envexpbot.2018.02.001

Mahalakshmi, S., Hema, N., Vijaya, P.P., 2020. In vitro biocompatibility and antimicrobial activities of zinc oxide nanoparticles (ZnO NPs) prepared by chemical and green synthetic route-a comparative study. BioNanoScience 10(1), 112-121. https://doi.org/10.1007/s12668-019-00698-w

Mandal, A.K., Katuwal, S., Tettey, F., Gupta, A., Bhattarai, S., Jaisi, S., *et al*., 2022. Current research on zinc oxide nanoparticles: synthesis, characterization, and biomedical applications. Nanomaterials 12(17), 3066. https://doi.org/10.3390/nano12173066

Mazhar, M.W., Ishtiaq, M., Maqbool, M., Ullah, F., Sayed, S.R. Mahmoud, E.A., 2023. Seed priming with iron oxide nanoparticles improves yield and antioxidant status of garden pea (*Pisum sativum* L.) grown under drought stress. S. Afr. J. Bot. 162, 577-587. https://doi.org/10.1016/j.sajb.2023.09.047

Methela, N.J., Pande, A., Islam, M.S., Rahim, W., Hussain, A., Lee, D.S., *et al*., 2023. Chitosan-GSNO nanoparticles: a positive modulator of drought stress tolerance in soybean. BMC Plant Biolog. 23(1), 639. https://doi.org/10.1186/s12870-023-04640-x

Monib, A.W., Niazi, P., Sediqi, S., 2023. Investigating approaches for optimizing agricultural yield: A comprehensive review of the crucial role of micronutrients in enhancing plant growth and maximizing production. J. Res. Appl. Sci. Biotechnol. 2(5), 168-180. https://doi.org/10.55544/jrasb.2.5.26

Movasaghi, Z., Rehman, S., ur Rehman, D.I., 2008. Fourier transform infrared (FTIR) spectroscopy of biological tissues. Appl. Spectrosc. Rev. 43(2), 134-179. https://doi.org/10.1080/05704920701829043

Nadeem, M., Li, J., Yahya, M., Sher, A., Ma, C., Wang, X., *et al.*, 2019. Research progress and perspective on drought stress in legumes: A review. Int. J. Mol. Sci. 20(10), 2541. https://doi.org/10.3390/ijms20102541

Ocieczek, A., Witczak, T., Witczak, M., 2025. Chemical composition and physical parameters of particles as factors of variability of the sorption properties of protein powder preparations. Int. Agrophys. 39(3), 255-267. https://doi.org/10.31545/intagr/200351

Olayinka, B.U., Abdulkareem, K.A., Murtadha, R.B., Abdulbaki, A.S., Ayinla, A., Sagaya, A., *et al*., 2021. Determination of chlorophyll content, carbonic anhydrase activity, bio-productivity and composition of groundnuts under five Zinc Oxide (ZnO) applications. Sri Lankan J. Biol. 6(1). https://doi.org/10.4038/sljb.v6i1.65

Pandey, J., Devadasu, E., Saini, D., Dhokne, K., Marriboina, S., Raghavendra, A.S., *et al*., 2023. Reversible changes in structure and function of photosynthetic apparatus of pea (*Pisum sativum*) leaves under drought stress. Plant J. 113(1), 60-74. https://doi.org/10.1111/tpj.16034

Patel, K.V., Nath, M., Bhatt, M.D., Dobriyal, A.K., Bhatt, D., 2020. Nanofomulation of zinc oxide and chitosan zinc sustain oxidative stress and alter secondary metabolite profile in tobacco. 3 Biotech.10(11), 477. https://doi.org/10.1007/s13205-020-02469-x

Priss, O., Hutsol, T., Glowacki, S., Bulhakov, P., Bakhlukova, K., Osokina, N., *et al*., 2024. Effect of asparagus chitosan-rutin coating on losses and waste reduction during storage. Agric. Eng. Polish Soc. Agric. Eng. 28(1), 99-118. https://doi.org/10.2478/agriceng-2024-0008

Queiroz, M.F., Teodosio Melo, K.R., Sabry, D.A., Sassaki, G.L. Rocha, H.A.O., 2014. Does the use of chitosan contribute to oxalate kidney stone formation?. Mar. Drugs. 13(1), 141-158. https://doi.org/10.3390/md13010141

Raja, V., Singh, K., Qadir, S.U., Singh, J., Kim, K.H., 2024. Alleviation of cadmium-induced oxidative damage through application of zinc oxide nanoparticles and strigolactones in *Solanum lycopersicum* L. Environ.Sci. Nano. 11(6), 2633-2654. https://doi.org/10.1039/D3EN00796K

Rani, N., Kusum, Hooda, V., 2024. Chitosan/ZnO nanocomposites for improving the growth and reducing the toxicity of Zn in *Sorghum bicolor* (L.) Moench plants. Acta Physiol. Plant. 46(6), 67. https://doi.org/10.1007/s11738-024-03693-1

Rani, S., Kumari, N., Sharma, V., 2023. Uptake, translocation, transformation and physiological effects of nanoparticles in plants. Arch. Agron. Soil Sci. 69(9), 1579-1599. https://doi.org/10.1080/03650340.2022.2103549

Raza, M.A.S., Muhammad, F., Farooq, M., Aslam, M.U., Akhter, N., Toleikienė, M., *et al*., 2025. ZnO-nanoparticles and stage-based drought tolerance in wheat (*Triticum aestivum* L.): effect on morpho-physiology, nutrients uptake, grain yield and quality. Sci. Rep. 15(1), 5309. https://doi.org/10.1038/s41598-025-89718-2

Rinaudo, M., 2006. Chitin and chitosan: Properties and applications. Prog. Polym. Sci. 31(7), 603-632. https://doi.org/10.1016/j.progpolymsci.2006.06.001

Roig-Oliver, M., Fullana-Pericàs, M., Bota, J., Flexas, J., 2021. Adjustments in photosynthesis and leaf water relations are related to changes in cell wall composition in *Hordeum vulgare* and *Triticum aestivum* subjected to water deficit stress. Plant Sci. 311, 111015. https://doi.org/10.1016/j.plantsci.2021.111015

Sachdev, S., Ansari, S.A., Ansari, M.I., Fujita, M., Hasanuzzaman, M., 2021. Abiotic stress and reactive oxygen species: Generation, signaling, and defense mechanisms. Antioxidants 10(2), 277. https://doi.org/10.3390/antiox10020277

Sadati, S.Y.R., Godehkahriz, S.J., Ebadi, A., Sedghi, M., 2022. Zinc oxide nanoparticles enhance drought tolerance in wheat *via* physio-biochemical changes and stress genes expression. Iran. J. Biotechnol. 20(1), e3027.

Sairam, R.K., Rao, K.V., Srivastava, G.C., 2002. Differential response of wheat genotypes to long term salinity stress in relation to oxidative stress, antioxidant activity and osmolyte concentration. Plant Sci. J. 163(5), 1037-1046. https://doi.org/10.1016/S0168-9452(02)00278-9

Saleem, M.H., Parveen, A., Perveen, S., Akhtar, N., Abasi, F., Ehsan, M., *et al*., 2024. Alleviation of cadmium toxicity in pea (*Pisum sativum* L.) through Zn-Lys supplementation and its effects on growth and antioxidant defense. Environ. Sci. Pollut. Res. 31(7), 10594-10608. https://doi.org/10.1007/s11356-024-31874-5

Seleiman, M.F., Ahmad, A., Alhammad, B.A., Tola, E., 2023. Exogenous application of zinc oxide nanoparticles improved antioxidants, photosynthetic, and yield traits in salt-stressed maize. Agronomy 13(10), 2645. https://doi.org/10.3390/agronomy13102645

Semida, W.M., Abdelkhalik, A., Mohamed, G.F., Abd El-Mageed, T.A., Abd El-Mageed, S.A., Rady, M.M., *et al*., 2021. Foliar application of zinc oxide nanoparticles promotes drought stress tolerance in eggplant (*Solanum melongena* L.). Plants. 10(2), 421. https://doi.org/10.3390/plants10020421

Shahab, H., Iqbal, M., Sohaib, A., Khan, F.U., Waqas, M., 2024. IoT-based agriculture management techniques for sustainable farming: A comprehensive review. Comput Electron Agric. 220, 108851. https://doi.org/10.1016/j.compag.2024.108851

Sharma, P., Jha, A.B., Dubey, R.S., 2025. Utilizing manganese-based nanoparticles for enhancing environmental stress resilience and productivity of plants. Environ. Sci. Nano. 12(5), 2580-2602. https://doi.org/10.1039/D5EN00292C

Sheteiwy, M.S., Shaghaleh, H., Hamoud, Y.A., Holford, P., Shao, H., Qi, W., *et al*., 2021. Zinc oxide nanoparticles: potential effects on soil properties, crop production, food processing, and food quality. Environ. Sci. Pollut. Res. 28(28), 36942-36966. https://doi.org/10.1007/s11356-021-14542-w

Simkin, A.J., Kapoor, L., Doss, C.G.P., Hofmann, T.A., Lawson, T., Ramamoorthy, S., 2022. The role of photosynthesis related pigments in light harvesting, photoprotection and enhancement of photosynthetic yield in planta. Photosynth. Res. 152(1), 23-42. https://doi.org/10.1007/s11120-021-00892-6

Singh, A., Rajput, V.D., Al Tawaha, A.R.M., Al Zoubi, O.M., Habeeb, T., Rawat, S., *et al*., 2023. A review on crop responses to nanofertilizers for mitigation of multiple environmental stresses. Ecol. Eng. Environ. Technol. 24. https://doi.org/10.12912/27197050/169313

Singh, A., Rajput, V.D., Lalotra, S., Agrawal, S., Ghazaryan, K., Singh, J., *et al*., 2024. Zinc oxide nanoparticles influence on plant tolerance to salinity stress: insights into physiological, biochemical, and molecular responses. Environ. Geochem. Health. 46(5), 148. https://doi.org/10.1007/s10653-024-01921-8

Singh, G.B., Sharma, A., Thapa, J., Nidhi, 2024. Foliar-Based nanoformulations: leads and flaws. In Metabolomics,

Proteomics and Gene Editing Approaches in Biofertilizer Industry: 2, 223-245. Singapore: Springer Nature Singapore. https://doi.org/10.1007/978-981-97-2910-4_12

Song, C., Yu, H., Zhang, M., Yang, Y., Zhang, G., 2013. Physicochemical properties and antioxidant activity of chitosan from the blowfly *Chrysomya megacephala* larvae. Int. J. Biol. Macromol. 60, 347-354. https://doi.org/10.1016/j.ijbiomac.2013.05.039

Sparks D.L., Page, A.L., Helmke, P.A., Loeppert, R.H., Soltanpour, P.N., Tabatabai, M.A., 1996. Methods of soil analysis: Part 3. Chemical methods. Soil Science Society of America, Inc., American Soc. Agron., Inc., Madison. https://doi.org/10.2136/sssabookser5.3

Stasińska-Jakubas, M., Hawrylak-Nowak, B., 2022. Protective, biostimulating, and eliciting effects of chitosan and its derivatives on crop plants. Molecules 27(9), 2801. https://doi.org/10.3390/molecules27092801

Suganya, A., Saravanan, A., Manivannan, N., 2020. Role of zinc nutrition for increasing zinc availability, uptake, yield, and quality of maize (*Zea mays* L.) grains: An overview. Commun. Soil Sci. Plant Anal. 51(15), 2001-2021. https://doi.org/10.1080/00103624.2020.1820030

Sun, L., Song, F., Zhu, X., Liu, S., Liu, F., Wang, Y., *et al*., 2021. Nano-ZnO alleviates drought stress via modulating the plant water use and carbohydrate metabolism in maize. Arch. Agron. Soil Sci. 67(2), 245-259. https://doi.org/10.1080/03650340.2020.1723003

Sun, X., Wang, H., Liang, H., Meng, N., Zhou, N., 2025. Fabrication of antimicrobial chitosan/ZnO nanoparticles/lecithin-montmorillonite films for food packaging application. Food Hydrocoll. 159, 110686. https://doi.org/10.1016/j.foodhyd.2024.110686

Teng, Z., Chen, Y., Meng, S., Duan, M., Zhang, J., Ye, N., 2023. Environmental stimuli: A major challenge during grain filling in cereals. Int. J. Mol. Sci. 24(3), 2255. https://doi.org/10.3390/ijms24032255

Vino, A.B., Ramasamy, P., Shanmugam, V., Shanmugam, A., 2012. Extraction, characterization and in vitro antioxidative potential of chitosan and sulfated chitosan from cuttlebone of *Sepia aculeata* Orbigny, 1848. Asian Pac. J. Trop. Biomed. 2(1), S334-S341. https://doi.org/10.1016/S2221-1691(12)60184-1

Wang, X., Xie, H., Wang, P., Yin, H., 2023. Nanoparticles in plants: uptake, transport and physiological activity in leaf and root. Materials 16(8), 3097. https://doi.org/10.3390/ma16083097

Wang, Z., Wang, S., Ma, T., Liang, Y., Huo, Z., Yang, F., 2023. Synthesis of zinc oxide nanoparticles and their applications in enhancing plant stress resistance: A review. Agronomy. 13(12), 3060. https://doi.org/10.3390/agronomy13123060

Yogamalar, R., Srinivasan, R., Vinu, A., Ariga, K., Bose, A.C., 2009. X-ray peak broadening analysis in ZnO nanoparticles. Solid State Commun. 149(43-44), 1919-1923. https://doi.org/10.1016/j.ssc.2009.07.043

Zaman, H.G., Baloo, L., Aziz, F., Kutty, S.R., Ashraf, A., 2022. COD adsorption and optimization from produced water using chitosan-ZnO nanocomposite. Appl. Nanosci. 12(6), 1885-1898. https://doi.org/10.1007/s13204-022-02392-y

Zulfiqar, F., Ashraf, M., 2023. Proline alleviates abiotic stress induced oxidative stress in plants. J. Plant Growth Regul. 42(8), 4629-4651. https://doi.org/10.1007/s00344-022-10839-3

Zulfiqar, F., Akram, N.A., Ashraf, M., 2020. Osmoprotection in plants under abiotic stresses: New insights into a classical phenomenon. Planta. 251(1), 3. https://doi.org/10.1007/s00425-019-03293-1